

---

# Removal of fluoride from groundwater using a zeolite A supported magnetite biochar composite

---

---

Received: 24 October 2025

Accepted: 2 December 2025

Published online: 20 January 2026

Cite this article as: Derbe T., Tesfaye Y., Sani T. *et al.* Removal of fluoride from groundwater using a zeolite A supported magnetite biochar composite. *Sci Rep* (2025). <https://doi.org/10.1038/s41598-025-31370-x>

Tessema Derbe, Yitayew Tesfaye, Taju Sani & Enyew Amare Zereffa

---

We are providing an unedited version of this manuscript to give early access to its findings. Before final publication, the manuscript will undergo further editing. Please note there may be errors present which affect the content, and all legal disclaimers apply.

If this paper is publishing under a Transparent Peer Review model then Peer Review reports will publish with the final article.

# Removal of Fluoride from Groundwater using a Zeolite A Supported Magnetite Biochar Composite

Tessema Derbe<sup>1</sup>, Yitayew Tesfaye<sup>2, 3</sup>, Taju Sani<sup>2, 3\*</sup>, and Enyew Amare Zereffa<sup>4</sup>

1 Department of Chemistry, Wachemo University, P.O. Box 667, Hossana, Ethiopia

2 Department of Industrial Chemistry, Addis Ababa Science and Technology University, P.O. Box 16417, Addis Ababa, Ethiopia.

3 Nanotechnology Center of Excellence, Addis Ababa Science and Technology University, P.O. Box 1647, Addis Ababa, Ethiopia.

<sup>4</sup>Department of Applied Chemistry, School of Applied Natural Science, Adama Science and Technology University, P.O. Box 1888, Adama, Ethiopia.

\* Correspondence: [taju.sani@aastu.edu.et](mailto:taju.sani@aastu.edu.et); +251-9-43-80-30-20

## Abstract

Prolonged consumption of excess fluoride concentration ( $>1.5 \text{ mg/L}$ ) from groundwater notably poses serious health effects, including dental and skeletal fluorosis in the Rift Valley area of Ethiopia. In this study, a zeolite A supported magnetite biochar composite (Z-A/M-BC) was synthesized through a pyrolysis method for the removal of fluoride from groundwater. The as-synthesized adsorbent was characterized using FT-IR, PXRD, SEM-EDX, PZC, and BET analysis to identify the functional group, phase structure, surface morphology, elemental composition, surface charge distribution, and surface area, respectively. The  $pH_{ZPC}$  determination for Z-A/M-BC is found to be 6.75, suggesting a large portion of the adsorbent with  $pH$  less than this value becomes protonated and positively charged and thus is favorable for fluoride removal through electrostatic attraction. Interestingly, the BET analysis results also exhibited that the synthesized Z-A/M-BC composite had a high surface area of  $496.17 \text{ m}^2/\text{g}$ , which is accessible for capturing fluoride from groundwater. The adsorption study was commenced via optimization of reaction parameters:  $pH$ , adsorbent dose, initial concentration ( $C_0$ ), and contact time. The highest fluoride removal efficiency (95.80%) and capacity (6.39 mg/g) were recorded at  $pH$  5, 1.2 g/L of adsorbent dose, 6 h of contact time, and 10 mg/L of  $C_0$ . The removal performance of the Z-A/M-BC composite was also tested in a real sample of

groundwater having 12.25 mg/L of fluoride  $C_o$  which was collected from Kenteri town, Ethiopia. It was found to be 88.98% removal efficiency and 7.27 mg/g capacity, respectively. At last, the reusability study was conducted for 5 successive runs and found 95.80%, 90.40%, 87.30%, 85.40%, and 70.20% removal efficiency for the first, second, third, fourth, and fifth cycles, respectively. These confirm that the Z-A/M-BC adsorbent is promising for the removal of fluoride from groundwater at a large scale.

**Keywords:** Adsorbent; Composite; Groundwater; Fluoride; Removal

## Introduction

Fluorine is well known for its high electron affinity and reactivity and is frequently found as fluoride ions. Fluoride is present in various minerals such as fluorite, fluorapatite, biotite, cryolite, and topaz [1]. Wastes discharged into surface and groundwater from various industries, such as fertilizer, electroplating, semiconductor, glass, and ceramics industries, also increase the amount of fluorides in surface and groundwater above the permissible level set by the World Health Organization (WHO) [2]. According to the WHO guidelines, the maximum acceptable limit of fluoride in drinking water is 0.5 to 1.5 mg/L [3]. Within the limit, fluoride is vital for the prevention of tooth decay and supports the proper growth of bone structure in human beings [1,4]. However, beyond the threshold limit, fluoride leads to various diseases, including skeletal and teeth fluorosis [3], joint stiffness [5], paralysis, thyroid dysfunction, and other gum diseases [1, 6, 7]. The problem spreads throughout the globe, specifically in many tropical and subtropical countries, including Libya, Iran, China, Iraq, South Africa, Kenya, and Ethiopia. In Ethiopia [7], particularly in the Rift Valley areas, the problem is getting worse. For instance, the research work conducted by Ebsa, G. [8] shows the high fluoride concentration ranging from 3.8 mg/L to 12.7 mg/L in the Ziway district. According to Fito, J., *et al.* report [9], the concentration of fluoride in the Rift Valley of Ethiopia also ranges from 5 to 26 mg/L, which is significantly higher than the limits set by WHO. Similarly, contemporary research conducted by Gómez-Hortigüela and his co-workers also confirms the presence of high fluoride concentrations ( $> 5$  mg/L) in the Rift Valley and lowland areas of Ethiopia [1]. Accordingly, reducing the fluoride concentration in potable water below WHO guidelines is being demanded and due substantial attention.

To date, numerous removal methods, including chemical precipitation [10], membrane separation [11,12], ion exchange [13], and adsorption [14], are widely used for the removal of fluoride. Most of them suffered with high costs, complicated procedures, usage of toxic chemicals, and low recovery [10, 14]. For instance, the chemical precipitation consumes large chemicals and generates secondary pollutant (sludge) which has adverse effects on human health and aquatic life [12,15]. An ion-exchange is vulnerable to the interference of other ions [16, 17]. Besides, it is relatively costly, and mostly limited on isoelectronic ions [14]. Membrane-based methods such as reverse osmosis, electrodialysis, and nanofiltration are highly effective for the removal of contaminates, however the method is complicated, costly, and suffers from membrane fouling, which is impractical for developing countries and rural areas [12, 18]. Consequently, adsorption is found to be desirable for developing countries owing to its cost-effectiveness, simplicity to operate, and environmental friendliness [1, 11, 15]. Moreover, it uses a wide range of adsorbent materials such as zeolite, activated carbon, biochar, polymer, hydroxyapatite, and metal-organic frameworks (MOFs) for the defluoridation of groundwater [6, 15, 16]. Herein, the Z-A/M-BC composite and its pristine adsorbents were tested for the removal of fluoride from groundwater.

Zeolites are crystalline aluminosilicates, which consist of aluminum and silicon atoms bonded through bridging oxygen atoms to adopt a tetrahedral framework ( $\text{TO}_4$ , T=Si, or Al) [17]. The structure and porosity (Fig. 1a) of zeolites provide a good occasion for further modification with suitable motifs to develop efficient adsorbents for various applications [1]. Zeolite-A (Z-A) is the most common zeolite family, having high Al content and high cationic exchanger ability [18]. Due to its extensive sources, stability, large surface area, and obtainability, Z-A is used for the adsorption of cationic pollutants like heavy metals [18]. However, Z-A has a net negative charge at the Al metal center (Fig. 1b), which rendered the application of Z-A for the removal of fluoride from contaminated water [1, 18,19] due to columbic repulsive force.

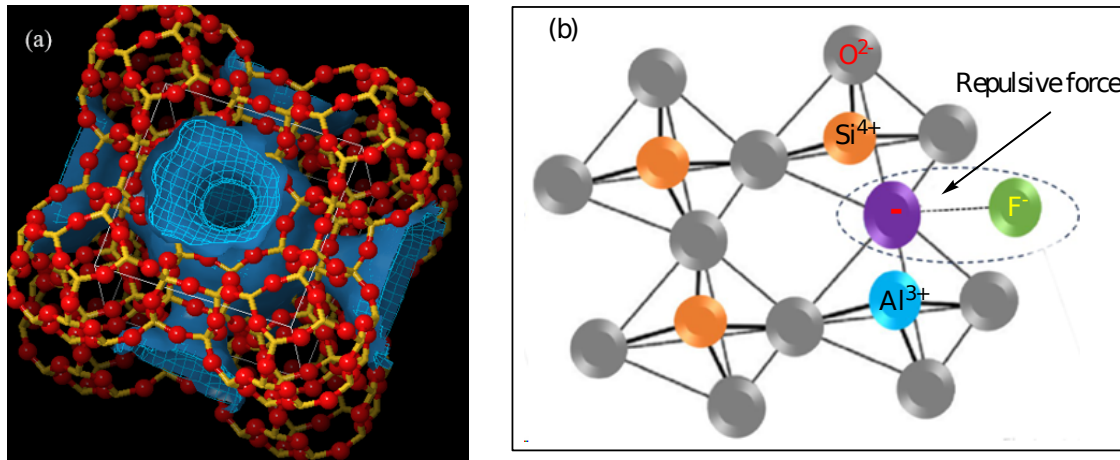


**Fig. 1** porosity of Z-A (a), and electrostatic repulsion between zeolite surface charge and fluoride (b) drawn by Adobe Photoshop [20].

Biochar (BC) is one of the most popular environmentally friendly and low-cost porous materials for the adsorption of pollutants [22, 23]. BC has received much attention owing to its high carbon content, surface-enriched chemistry, and stable structure [12, 19, 20]. Nevertheless, it possesses disordered structures, non-uniform sizes, and lacks recyclability, which creates secondary pollutants after adsorption [13, 22]. These downsides will greatly limit the applications of BC for the removal of fluoride, which needs magnetization with magnetic materials. Magnetite ( $\text{Fe}_3\text{O}_4$ ) is an inverted spinel possessing high chemical stability, high coercivity, excellent chelation behavior, and high selectivity towards fluoride adsorption [20, 23]. Thus, designing adsorbent materials with high adsorption efficiency and recyclability is highly demanded.

In the present study, a Z-A/M-BC composite was synthesized for the removal of fluoride from groundwater. In the Z-A/M-BC composite, Z-A provides structural stability of the synthesized adsorbent [18];  $\text{Fe}_3\text{O}_4$  enhances the recovery and the defluoridation efficiency of the Z-A/M-BC composite. BC also conveys the functionality and active sites for fluoride removal in Z-A/M-BC composite. Thus, compositing Z-A and M-BC enhances the defluoridation efficiency of Z-A/M-BC composite. The defluoridation studies were commenced by optimization of sorption factors such as pH, adsorbent dose,  $C_0$ , and adsorption time. Besides, the Box-

Behnken model was also applied using Design Expert 13 software to study the mutual interaction effects of contact time,  $C_0$ , and adsorbent dose during defluoridation of groundwater.

## Materials and Method

### Chemicals and Reagents

Analytical graded chemicals:  $\text{FeCl}_2 \cdot 4\text{H}_2\text{O}$ , 99% and  $\text{FeCl}_3 \cdot 6\text{H}_2\text{O}$ , 97% was supplied by Sisco Research Laboratories Pvt. Ltd., Delhi, India.  $\text{C}_2\text{H}_6\text{O}$  (96%, *Sigma-Aldrich*),  $\text{NaOH}$  (98%, *Merck*), DMF (99%, *Merck*),  $\text{CH}_3\text{COOC}_2\text{H}_5$  (99%, *Merck*),  $\text{HCl}$  (37%, *Sigma-Aldrich*),  $\text{NaCl}$  (99.5%, *Maharashtra, India*),  $\text{Na}_3\text{C}_6\text{H}_5\text{O}_7 \cdot 2\text{H}_2\text{O}$  (98%, *UDYOG, India*),  $\text{C}_2\text{H}_4\text{O}_2$  (99.8%, *Pentokey Organy, India*), and  $\text{NaF}$  (99%, *Sigma-Aldrich*) were obtain from central laboratory, AASTU, Ethiopia. The corn (source of corn cob) was purchased from a street market in Addis Ababa city, Ethiopia. Furthermore, kaolin was collected from western Homa near Hossana, Ethiopia, which was used as raw material for the synthesis of Z-A. Groundwater sample was collected from Kenteri town, Bora woreda, Ethiopia.

### Instruments

The phase structural and crystallinity of the synthesized adsorbent was examined by X-Ray Diffraction Spectroscopy (XRD, *Bruker-AXS D8, Advance Type*,) at  $\text{Cu k}\alpha$  radiation ( $\lambda = 1.54 \text{ \AA}^\circ$ , 40 kV, 44 mA). The functional groups were analyzed using Transform-Infrared Spectroscopy (*FT-IR, iS50 ABX, Germany*). The surface area of synthesized adsorbent was scrutinized using Brunauer-Emmett-Teller (BET, *Quantachrome AUTOSORB-1, USA*). The surface morphology and elemental composition of synthesized adsorbent were also characterized by Scanning Electron Microscopy coupled with energy dispersive spectroscopy (*SEM-EDS, JEOL JSM-6500F, Japan*). The concentration of fluoride was measured using fluoride ion selective electrode (*Metrhom-6.0502.150, Germany*).

### Adsorbent Synthesis

#### Synthesis of magnetite ( $\text{Fe}_3\text{O}_4$ )

The  $\text{Fe}_3\text{O}_4$  was synthesized through the co-precipitation method [24] at a 2:1 molar ratio of  $\text{FeCl}_3 \cdot 6\text{H}_2\text{O}$  to  $\text{FeCl}_2 \cdot 4\text{H}_2\text{O}$  using as a precursor and  $\text{NaOH}$  as a

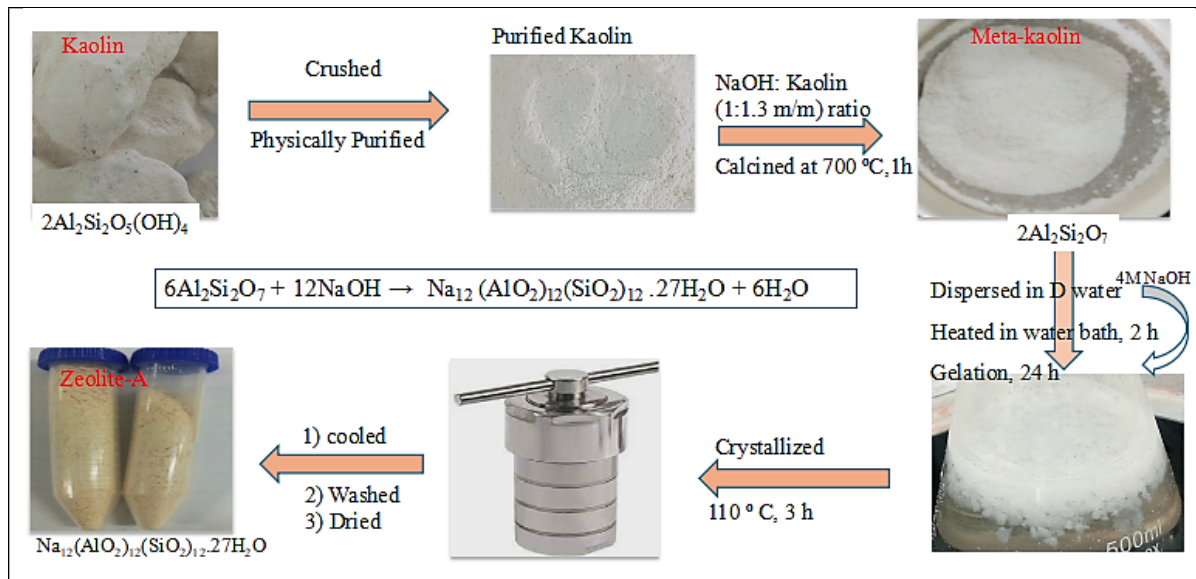
precipitating agent. To describe briefly: 4 g of  $\text{FeCl}_2 \cdot 4\text{H}_2\text{O}$  and 8 g of  $\text{FeCl}_3 \cdot 6\text{H}_2\text{O}$  were dissolved in 180 mL of distilled water and stirred for 2 h at 70 °C. The 4 M NaOH solution was added dropwise into the solution till the pH reached 10 [20, 25]. The solution was allowed for 12 h to precipitate at room temperature. The precipitate was separated via magnetic bar and washed with distilled water and acetone [20, 26]. Hereafter, the precipitate was oven-dried at 60 °C for 6 h.

#### Synthesis of BC and M-BC composite

Initially, the BC was synthesized through pyrolysis of corn cobs according to the procedure [27, 28] with a little bit of modification. The corn cob was dried and crushed into powder. 5 g of powder was pyrolyzed in a muffle furnace at 450 °C for 3 h under a 5 °C min<sup>-1</sup>  $\text{N}_2$  gas flow rate [29]. Afterward, the BC was ground and sieved using 100 mm Mesh sieve. Secondly, the BC was magnetized by dispersing 10 g of BC in 200 mL of distilled water with continuous stirring for 30 min [30]. In another beaker, 7 g of  $\text{FeSO}_4 \cdot 7\text{H}_2\text{O}$  and 14 g of  $\text{FeCl}_3 \cdot 6\text{H}_2\text{O}$  were dissolved in 100 mL of distilled water and stirred for 1 h at 60 °C. This solution was transferred into BC suspension and stirred for another 1 h at 60 °C. Then, 4 M of NaOH solution was added dropwise at ambient temperature to adjust the pH to 10 [25]. Then, the solution was allowed 12 h to co-precipitate. The precipitate was collected by magnetic bar and dried for 12 h at 60 °C.

#### Synthesize of Z-A

Z-A was synthesized through the hydrothermal method according to the procedure reported previously [18, 20]. To describe briefly: 40 g of raw kaolin was soaked with 400 mL of distilled water for 4 days with continuous stirring. The suspension was centrifuged and dried. The treated kaolinite was calcined at 700 °C for 3 h. Fine powder metakaolin was treated with 4 M NaOH-hot water (1:5 m/v ratio) and heated in a water bath for 1 h at 70 °C for gel formation (Scheme 1). The gel was aged for 12 h at room temperature and heated at 110 °C for 12 h in a Teflon-lined steel autoclave. The product was centrifuged, washed many times with deionized water, and dried in an oven at 80 °C.



**Scheme 1** Synthesis of Z-A through hydrothermal method.

#### Synthesis of Z-A/M-BC composite

Z-A/M-BC composite was synthesized by the pyrolysis method [18,31]. Typically: 3.6 g of Z-A and 7.2 g of M-BC were dispersed in 150 mL of deionized water [32]. The mixture was stirred for 3 h and allowed to react at ambient temperature for 24 h. The suspension was centrifuged and dried at 80 °C in an oven for 6 h [26]. The dried solid was pyrolyzed (5 °C/min) at 450 °C for 3 h [33]. The crucible was desiccated and the resulting composite material was ground.

#### Adsorption Studies

##### Determination of zero-point charge (pH<sub>zpc</sub>)

The zero-point charge of Z-A/M-BC absorbent was investigated at 3, 5, 7, 9, and 11 pH using 0.5 M HCl and 0.05 M NaOH [20, 34]. 1.5 g of the synthesized adsorbent was added into each 50 mL of the pre-pH adjusted solution. The solution was shaken for 90 min using an orbital shaker and allowed for 20 h. Hereafter, the adsorbent was separated by an external magnetic bar and the pH values of each filtrate were recorded. The pH<sub>ZPC</sub> of the adsorbents was identified from a common intersection point of the curve of initial pH and their corresponding ΔpH change [35].

#### Parameters optimization

Firstly, ionic strength adjustment buffer type I (TISAB-I) was prepared according to the procedures reported by Gao, Y. *et al.* and Teju, M. *et al.* [7,20,

36]. To describe briefly: 58 g of NaCl and 7 g of Na<sub>3</sub>C<sub>6</sub>H<sub>5</sub>OH.nH<sub>2</sub>O were dissolved in 500 mL distilled water. And then 57 mL CH<sub>3</sub>COOH was added to the solution. The pH of solution was maintained to 5.3 using 0.5 M NaOH. The standard solutions (2, 4, 6, 10, and 14 mg/L) were also prepared through serial dilution from the stock solution for sketching of the calibration curve (Fig. S1). Then after, the removal study was commenced by optimizing the removal parameters such as pH, adsorbent dose, C<sub>o</sub>, and contact time [3, 16, 37].

The impact of pH on the removal test was studied at pH values of 3, 5, 7, 9, 11, and 13 using 0.05 M HCl and 0.05 M NaOH solutions at 1.5 g/L of adsorbent dose, 10 mg/L of C<sub>o</sub>, and 6 h of contact time [35]. The effect of C<sub>o</sub> was examined at 5, 10, 15, 20, 30, and 40 mg/L [9] (contact time = 6 h, pH = 5, adsorbent dose = 1.5 g/L). The effect of adsorbent dose on fluoride removal efficiency was studied at adsorbent doses of 0.5, 1, 1.5, 2, and 2.5 g/L (C<sub>o</sub> = 10 mg/L, contact time = 6 h, pH = 5). The impact of contact time was also studied by varying the adsorption time from 3 to 15 h (3, 6, 9, 12, 15 h) at a pH of 5, 1.5 g/L of adsorbent dose, and 10 mg/L of C<sub>o</sub>. The mixture was shaken at 160 rpm for 90 min, equilibrated for 6 h, and then separated by an external magnet. After a while, 10 mL of TISAB was added to a polyethene bottle containing 20 mL filtrate, and the removal test was measured using FISE [20,38]. A real water sample analysis was also carried out by taking groundwater having 12.25 mg/L an C<sub>o</sub> from Kenteri town, Bora Woreda, Ethiopia, at confined conditions. The removal capacity (Q<sub>e</sub>), and efficiency (R) were evaluated using Equations (1) and (2), respectively [9,20].

$$Q_e = \frac{(C_o - C_e)V}{W}$$

(1)

$$\%R = \frac{(C_o - C_e)}{C_o} \times 100\%$$

(2)

Where, C<sub>o</sub> and C<sub>e</sub> represent the initial and equilibrium fluoride concentration (mg/L), respectively, V (mL) is the volume of solution, W (g) is the amount of the adsorbent.

#### Reusability test

The reusability of Z-A/M-BC was commenced by dispersing of fluoride exhausted adsorbent in 50 mL of 0.05 M NaOH solution and was shaken using an orbital shaker at 160 rpm for 90 min for desorption of fluoride [20, 39]. The adsorbent was

separated and an oven dried at 60 °C overnight. Thereafter, the activated Z-A/M-BC was reused for five successive removal tests at optimum conditions (contact time = 6 h, pH = 5, adsorbent dose = 1.5 g/L,  $C_0$  = 10 mg/L).

## Results and Discussion

### Characterization of Adsorbents

#### PXRD analysis

The PXRD peak in the range of  $2\theta = 10\text{--}30^\circ$  was observed, which confirms the formation of amorphous BC (Fig. 2a). The PXRD peaks for  $\text{Fe}_3\text{O}_4$  at  $2\theta = 30.33^\circ$ ,  $35.53^\circ$ ,  $43.42^\circ$ ,  $57.08^\circ$ , and  $63.02^\circ$  corresponded to (220), (311), (440), (511), and (440) the lattice planes, respectively (Fig. 2a). This result closely coincided with PXRD data reported by [20, 40] and verified the formation of  $\text{Fe}_3\text{O}_4$ . The broad peak from  $20\text{--}30^\circ$  and at  $18.36^\circ$ (111),  $30.33^\circ$ (220),  $35.47^\circ$ (311),  $43.02^\circ$ (400),  $57.14^\circ$ (511), and  $62.59^\circ$ (440) indicate the coexistence of  $\text{Fe}_3\text{O}_4$  and BC in the M-BC composite (Fig. 2a); the peak location of  $\text{Fe}_3\text{O}_4$  did not alter after loading of  $\text{Fe}_3\text{O}_4$  onto BC [20, 31]. Besides, the presence of new peaks at  $7.16^\circ$ ,  $10.16^\circ$ ,  $13.92^\circ$ , and  $21.71^\circ$  suggests the formation of new interactions between  $\text{Fe}_3\text{O}_4$  and BC in the M-BC composite [18,20]. The existence of a peak at  $2\theta = 30^\circ$  indicated the existence of Z-A, which played a major role in the Z-A/M-BC composite formation [26]. Besides, the PXRD peaks of  $\text{Fe}_3\text{O}_4$  and M-BC also appeared in their composite Z-A/M-BC composite, demonstrating the co-occurrence of Z-A and M-BC in the Z-A/M-BC composite material (Fig. 2b). Additionally, the occurrence of an intensified peak at  $23.72^\circ$  indicated the strong interaction between Z-A and M-BC, while the presence of new peaks at  $69.10^\circ$  and  $77.42^\circ$  suggested the formation of new bonds between Z-A and M-BC in the Z-A/M-BC adsorbent [41].

The average particle size of the Z-A/M-BC composite was estimated [20, 42] using Scherer's Equation (3) and found to be 27.98 nm. The BET result also indicates the porous nature of the synthesized Z-A/M-BC adsorbent with  $496.17\text{ m}^2/\text{g}$  surface area and  $0.08936\text{ cm}^3/\text{g}$  pore volume (Fig. S2 and Table S1).

$$D = \frac{k\lambda}{\beta \cos \theta} \quad (3)$$

Where  $D$  is the crystallites' size,  $k$  is Scherer's constant depending on the shape of particles (0.94),  $\lambda$  wavelength of the X-ray radiation (0.15418 nm for  $\text{CuK}\alpha$ ),  $\theta$  is the full width of half maximum (FWHM) intensity (in degree which converted to radian), and  $\theta$  is the diffraction (Bragg) angle.

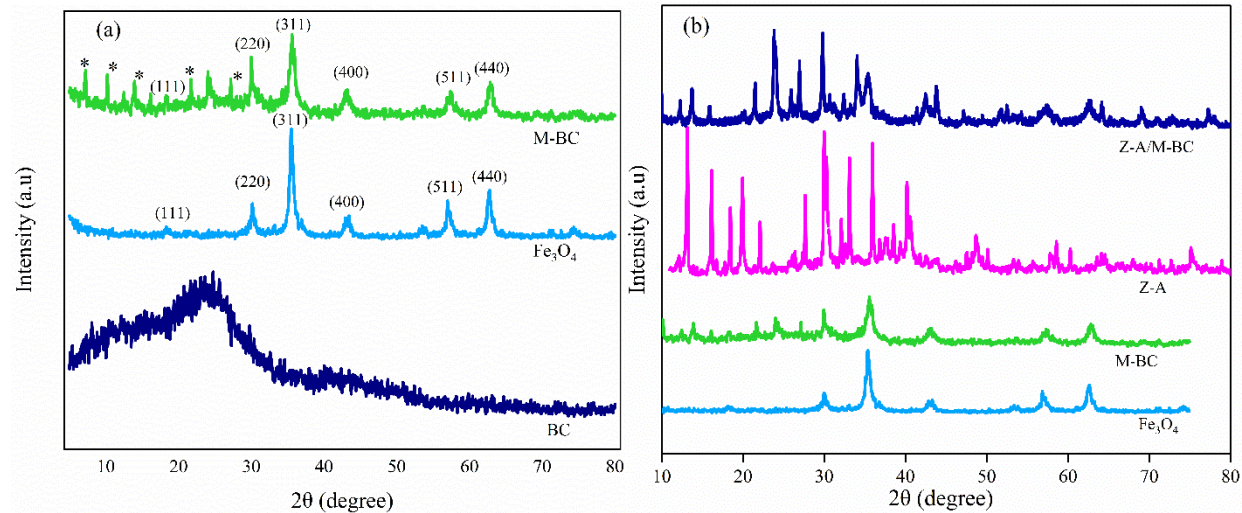


**Fig. 2** PXRD results of synthesized adsorbents.

#### FT-IR analysis

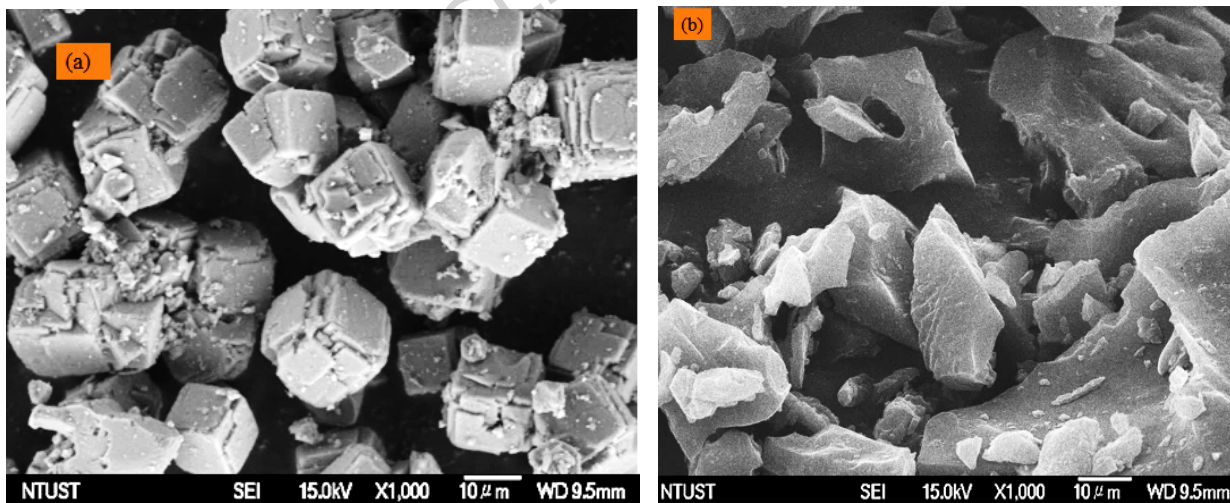
The representative peak of BC at  $3209\text{ cm}^{-1}$  corresponded to the -OH stretching vibration, which is ascribed to water molecules [43]. Peaks at  $3040$  and  $2912\text{ cm}^{-1}$  are attributed to stretching variations of =C-H and -C-H (Fig. S3a), respectively [18, 29]. Peaks at  $1574$  and  $1157\text{ cm}^{-1}$  correspond to C=C stretching variations in aromatic groups and C-O stretching vibration, sequentially [41]. Peaks at  $871$ ,  $805$ , and  $750\text{ cm}^{-1}$  reveal the existence of inorganic impurities (Si-O/Fe-O bonds), which are already shown in the EDX result (Fig. 4a). Peaks at  $971$  and  $781\text{ cm}^{-1}$  are attributed to the symmetric and asymmetric vibration bands of the  $\text{TO}_4$  tetrahedron (Fig. S3b) (where  $\text{T} = \text{Si}$  or  $\text{Al}$ ), respectively [26]. Wavenumbers at  $542$  and  $458\text{ cm}^{-1}$  are attributed to asymmetric external and symmetric internal vibrations of the double ring of Si and Al  $\text{TO}_4$  [18, 44]. Wavenumbers around  $3400$  and at  $1648\text{ cm}^{-1}$  suggested the stretching and bending vibration of  $\text{H}_2\text{O}$  molecules in the Z-A framework, respectively [45].

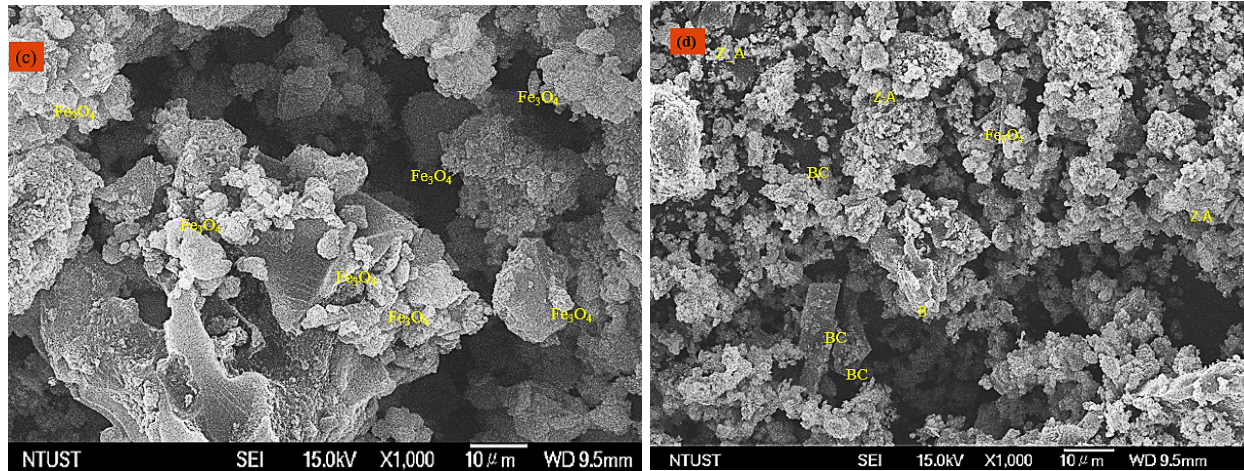
The FT-IR peaks at  $430$ ,  $538$ ,  $794$ , and  $889\text{ cm}^{-1}$  are attributed to Fe-O bond formation in  $\text{Fe}_3\text{O}_4$ . Wavenumbers at  $1629$  and  $3367\text{ cm}^{-1}$  also signify the bending and stretching vibration of the -OH on the surface of  $\text{Fe}_3\text{O}_4$  sequentially (Fig. S3c).

The FT-IR peak at  $580\text{ cm}^{-1}$  (Fe-O) in the M-BC composite also confirmed the presence of  $\text{Fe}_3\text{O}_4$  in the modified M-BC composite [40]. Attenuation of -OH intensity in the M-BC composite (Fig. S3d) proved the importance of hydrogen bonding in M-BC composite formation [31]. The prominent peak of Z-A/M-BC at  $1438\text{ cm}^{-1}$  is ascribed to the symmetric stretching vibration of the carboxylate ion. Peaks around 3357 and at  $1638\text{ cm}^{-1}$  corresponded to the stretching and bending vibration of O-H sequentially. The peak at  $2359\text{ cm}^{-1}$  is associated with the C-O stretching vibration [46]. Peaks at 972, 553, and  $488\text{ cm}^{-1}$  reveal the presence of M-O bonds (M = Si, Fe, Al) (Fig. S3d).

### SEM analysis

The SEM images of synthesized adsorbents were shown in Fig. 3a-d. The SEM result of Z-A revealed the presence of a cubic crystal structure with a size in the  $0.565\text{-}4.25\text{ }\mu\text{m}$  range (Fig. 3a). The SEM image of pristine BC is noticed to be rough and irregular with average sizes of  $8.74\text{ }\mu\text{m}$  (Fig. 3b). The SEM image of the M-BC composite shows them stuck to each other because of the presence of large surface energy [44] and spherical-shaped particles of  $\text{Fe}_3\text{O}_4$  (Fig. 3c). The average size of M-BC was found to be  $0.47\text{ }\mu\text{m}$ . The SEM image of Z-A/M-BC (Fig. 3d) is observed as nearly spherical with an average size of  $0.098\text{ }\mu\text{m}$  [47].

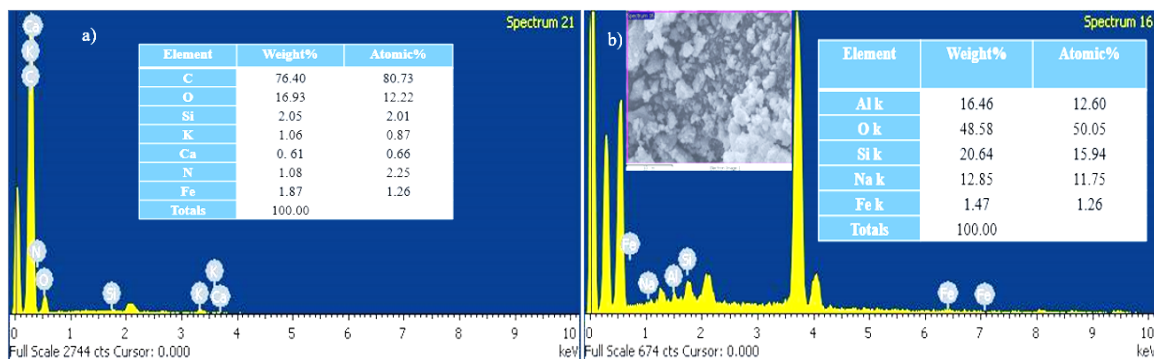




**Fig. 3** SEM images of Z-A (a), BC (b), M-BC (c) and Z-A/M-BC (d).

#### EDX results

The EDX band of pristine BC contains the anticipated elements of C and O, which are the main components of a distinctive BC material (Fig. 4a). The %weight of elemental composition of Z-A is found to be 20.84% Si, 17.46% Al, 48.58% O, and 12.85% Na, which confirms the purity of the synthesized material (Fig. 4b). As anticipated, the ratio of Si/Al for the as-synthesized Z-A was found to be 1.19, which is close to 1. This is further used to support the formation of pure Z-A [20]. The M-BC adsorbent encompasses 52.28% C, 22.07% O, 4.78% Al, 5.90% Si, 1.97% Ca, and 12.49% Fe [18] as it demonstrated in Fig. 4c. The anticipated elemental compositions of the Z-A/M-BC composite were found to be 47.25% C, 31.55% O, 3.03% Na, 2.62% Al, 3.65% Si, and 11.88% Fe (Fig. 4d). The elemental mapping distribution of synthesized adsorbents was illustrated in Fig. S4.



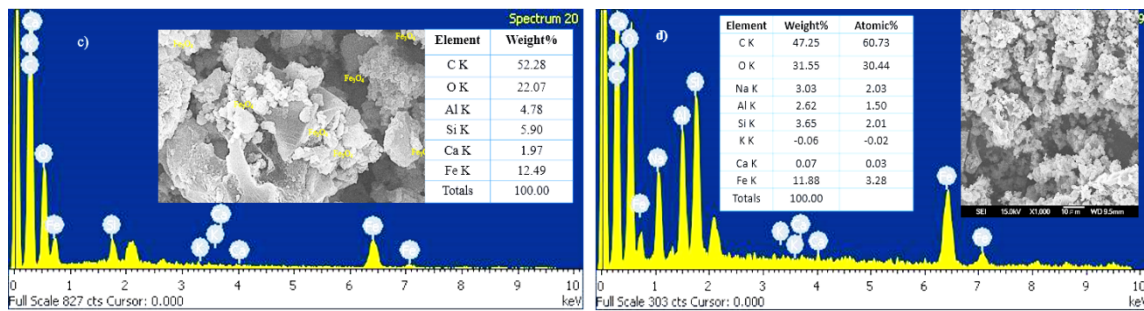


**Fig. 4** Elemental analysis of BC (a), Z-A (b), M-BC (c), and Z-A/M-BC (d).

### Adsorption Study

#### Determination of zero-point charge

In this work, the surface zero-point charge of Z-A/M-BC is determined and found to be 6.75 (Fig. 5). In this regard, when the solution pH is less than the pHZPC values, the net surface charge of the synthesized adsorbent becomes protonated and positively charged, having a greater attraction with fluoride. When the pH is above the PZC value, the surface of synthesized adsorbents is deprotonated (hydroxyl groups developed), which results in low removal capacity owing to their electrostatic repulsion force [18, 20].

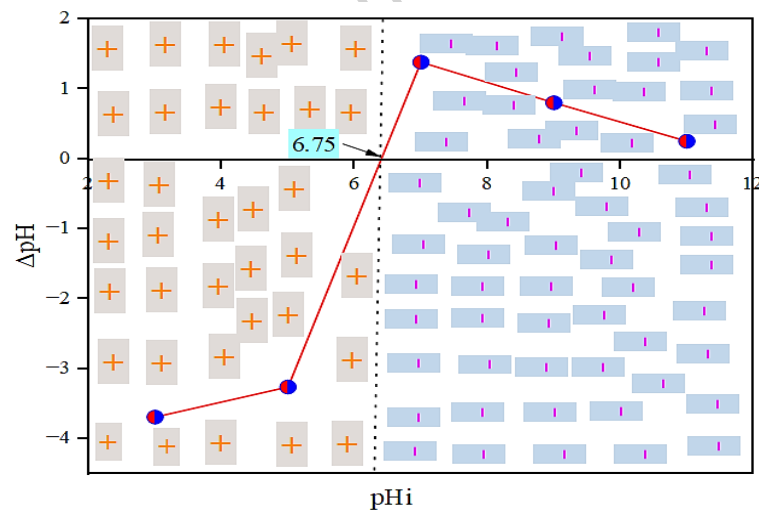


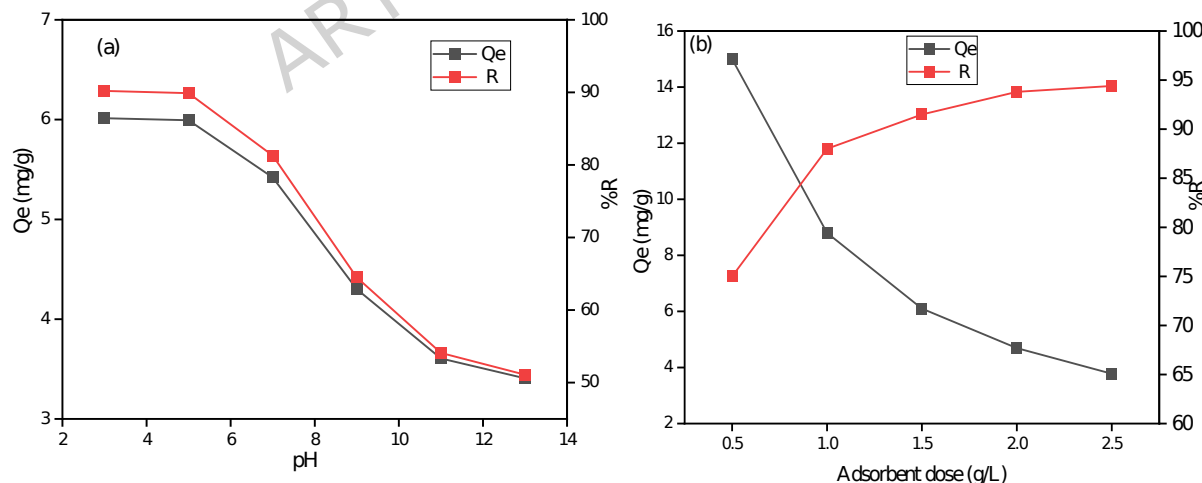
**Fig. 5** Zero-point charge of Z-A/M-BC composite.

#### Adsorption factors

The impact of pH on fluoride removal efficiency was investigated at different pH values (3, 5, 7, 9, 11, and 13) and resulted in 90.20%, 89.90%, 81.30%, 64.50%, 54.10%, and 51.10%, respectively (Fig. 6a). The highest removal efficiency was

obtained at pH of 3 and 5, respectively. However, pH 3 is inadequate for the practical removal of fluoride from groundwater. To offset this, all fluoride removal tests were conducted nearly neutral (pH = 5). After a while, the removal efficiency is decreased due to competition between OH<sup>-</sup> and fluoride ions for adsorption sites and coulombic repulsion force. The removal efficiency of Z-A/M-BC was found to be 75.00%, 88.91%, 91.50%, 93.80%, and 94.40% at 0.5, 1.0, 1.5, 2, and 2.5 g/L adsorbent doses (Fig. 6b), respectively, which increased with adsorbent dose. This is possibly due to the increment of free active sites on the adsorbent surface [1, 48]. Nevertheless, the removal efficiency shows a negligible increment after 1.5 g/L; this may be due to the saturation of adsorbent sites [48].

The influence of C<sub>0</sub> on the removal efficiency of Z-A/M-BC was executed at 5, 10, 15, 20, 30, and 40 mg/L and resulted in 83.60%, 92.80%, 90.53%, 78.75%, and 67.63%, respectively (Fig. 6c). The maximum adsorption efficiency (92.20%) was attained at 10 mg/L C<sub>0</sub> of fluoride. However, exceeding 10 mg/L, the removal efficiency decreased. This may be due to the competition among adsorbates for fixed active sites of the synthesized adsorbent [20]. The removal efficiency of Z-A/M-BC was found to be 80.30%, 92.20%, 93.10%, 93.80%, and 95.60% at contact time of 3, 6, 9, 12, and 15 h, respectively (Fig. 6d). The adsorption efficiency shows a slow increment after the optimum adsorption time (6 h). Consequently, the adsorption efficiency of synthesized increased contact time [1,16,50].



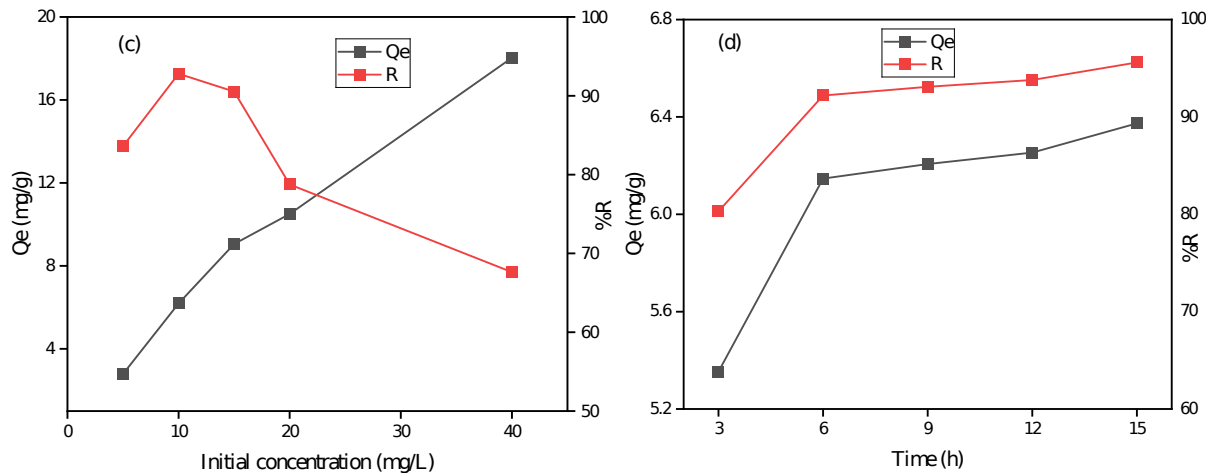


**Fig. 6** Impacts of (a) pH, (b) adsorbent dose,  $C_0$  (c), and contact time (d) on removal efficiency and capacity of Z-A/M-BC composite.

#### Adsorption isotherms

The adsorption isotherm is used to indicate whether the adsorbent surface is homogeneous or heterogeneous in which the adsorbate molecules are distributed over the surface [1]. The adsorption isotherm was tested using the Langmuir and Freundlich isotherms (Fig. 7). The linear form of Langmuir and Freundlich isothermal models were displayed using Equations (4) and (5), respectively [19,39].

$$\frac{C_e}{Q_e} = \frac{1}{K_L Q_m} + \frac{C_e}{Q_m} \quad (4)$$

$$\log Q_e = \log K_F + \frac{1}{n} \log C_e \quad (5)$$

where  $C_e$  is the equilibrium concentration of  $F^-$  in the solution (mg/L);  $Q_e$  is the amount of fluoride adsorbed per unit weight of Z-A/M-BC (mg/g),  $Q_m$  is the maximum adsorption capacity (mg/g) and  $K_L$  is the Langmuir constant related to energy (L/mg),  $K_F$  and  $n$  are dimensionless constants which are relative adsorption capacity and intensity of adsorption, respectively.

The values of  $Q_m$  and  $K_L$  of the linear expression of the Langmuir adsorption isotherm were calculated from the slope and intercept of the linear plot of  $C_e$  versus  $C_e/Q_e$ . The small values of  $K_L$  (0.2754 L/mg) indicate the weak interaction of

adsorbate with the Z-A/M-/BC surface. Besides, the low value of ( $R^2 = 0.86777$ ) doesn't explain the defluoridation activities adequately. In the Freundlich adsorption isotherm, the values of  $1/n$  (0.4829) lying between 0.1 and 1.0 and  $n$  (2.071) lying in  $10 > n > 1$  (Table S2) imply that the adsorption of fluoride on the Z-A/M-BC surface is privileged. Nevertheless, the values of KF and  $R^2$  were found to be 5.416 mg/g and 0.6334, respectively [39], which is far from the model. Unfortunately, neither the Langmuir nor the Freundlich isotherm model was well fit to express the defluoridation activities.

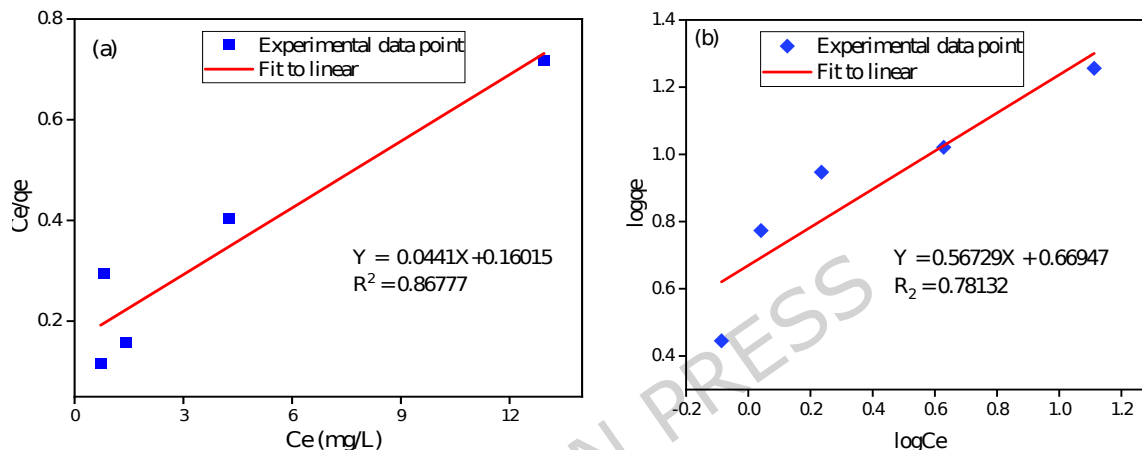


**Fig. 7** Langmuir adsorption isotherm model (a), and Freundlich adsorption isotherm model (b).

### Kinetic Models

The pseudo-first-order and pseudo-second-order use to familiar with the adsorption mechanisms and adsorption rate [51]. The fitness of pseudo-first order and pseudo-second order were evaluated using Equations (6) and (7), respectively.

$$\text{pseudo - first order : } \log(Q_e - Q_t) = \log Q_e - \frac{K_1 t}{2.303} \quad (6)$$

$$\text{pseudo - second order : } \frac{t}{Q_t} = \frac{1}{m K_2 Q_e} + \frac{t}{Q_e} \quad (7)$$

where  $Q_e$  is the amount of fluoride adsorbed per unit weight of Z-A/M-BC at equilibrium (mg/g),  $Q_t$  is the amount of fluoride adsorbed per unit weight of Z-A/M-

BC (mg/g) at time  $t$  (min), and  $k_1$  and  $k_2$  is the first and second pseudo-order rate constant for the adsorption ( $\text{min}^{-1}$ ), respectively.

The sketch of  $\log (Q_e - Q_t)$  against time (Fig. 8a) gives a linear relationship of the pseudo-first-order rate. The correlation factor ( $R^2$ ) of both pseudo-first-order (0.9515) and pseudo-second-order kinetics (0.999) are fitted (Table S3). However, the pseudo-first-order model is not appropriate to describe the adsorption kinetics since the theoretical adsorption capacity ( $Q_m \text{ fit} = 4.44 \text{ mg/g}$ ) was far from the experimental value ( $Q_m \text{ exp.} = 6.147 \text{ mg/g}$ ). On the other side, the linear plot of  $t/Qt$  versus time shows a higher coefficient ( $R^2 = 0.999$ ) for the pseudo-second-order kinetic model (Fig. 8b). Furthermore, the theoretical adsorption capacity ( $Q_m \text{ fit} = 6.62 \text{ mg/g}$ ) was closer to the experimental adsorption capacity ( $Q_m \text{ exp.} = 6.147 \text{ mg/g}$ ). Thus, the adsorption process best obeys the pseudo-second-order kinetic model in which the removal of fluoride is primarily controlled by chemisorption processes such as chemical precipitation, hydrogen bonding, ion exchange, and electrostatics [18,20].

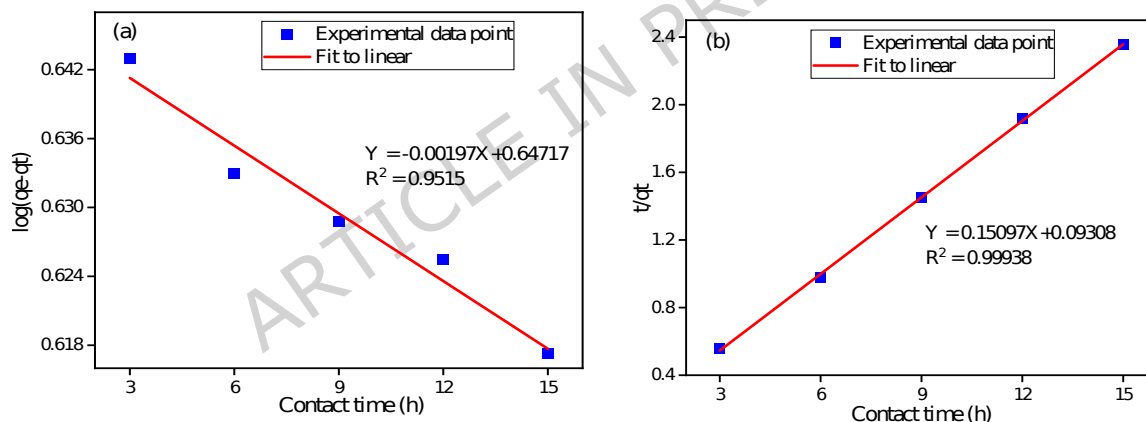


**Fig. 8** Pseudo-first-order kinetics model (a), and pseudo-second-order kinetics model (b).

#### Response surface method (RSM) study

The mutual interaction impacts of defluoridation parameters (contact time,  $C_o$ , and adsorbent dose) were also detected (at 17 runs) using the Box-Behnken model (Table S4) at constant  $\text{pH} = 5$ . Hereafter, the response and the input variables are expressed using a quadratic model-coded Equation (8).

$$\begin{aligned}
 \%R = & 86.57 + 1.924A - 3.35B + 1.20C + 1.06AB + 860AC + 0.1550BC - 0.625A^2 \\
 & - 0.3125B^2 \\
 & + 0.2475C^2
 \end{aligned} \tag{8}$$

Where, A, B, and C are the coded values of the operation variables for adsorbent dose,  $C_o$ , and contact time, respectively.

The model fitness was checked based on the values of the coefficient of determination ( $R^2$ ). The proximity of  $R^2$  value to unity ( $R^2 = 0.9973$ ), and the intimacy of adjusted ( $R^2 \text{ adj} = 0.9939$ ) and predicted  $R^2$  ( $R^2 \text{ pred} = 0.9574$ ) values to each other with the difference  $< 0.2$  suggest the fitness of model [18]. The predicted  $R^2$  value is reasonably agreed with the adjusted  $R^2$  value, which approves the model's fitness (Table S5). Besides, the precision that measures the signal-to-noise ratio ( $AP = 65.34$ ) is greater than 4; indicating a good signal and accurate model fit [18]. The F-value of 291.61 suggests that the model is significant. The P-values  $< 0.0500$  indicate the significance of the model. In this regard, A, B, C, AB, AC, and  $A^2$  are significant (Table S5). Consequently, the Box-Behnken model was verified and statistically proved to be reliable and adequate in defluoridation of drinking water.

The mutual impacts of contact time and  $C_o$  exhibited a positive effect on the defluoridation efficiency (Fig. 9). But individually, the  $C_o$  showed negative effects whereas the contact time showed a positive impact on the removal of fluoride [18]. The mutual interaction impacts of Z-A/M-BC dose and contact time on the removal of fluoride showed positive effects (Fig. 10). The collaboration of adsorbent dose and  $C_o$  of fluoride (Fig. 11) also shows favorable effect on the removal of fluoride.

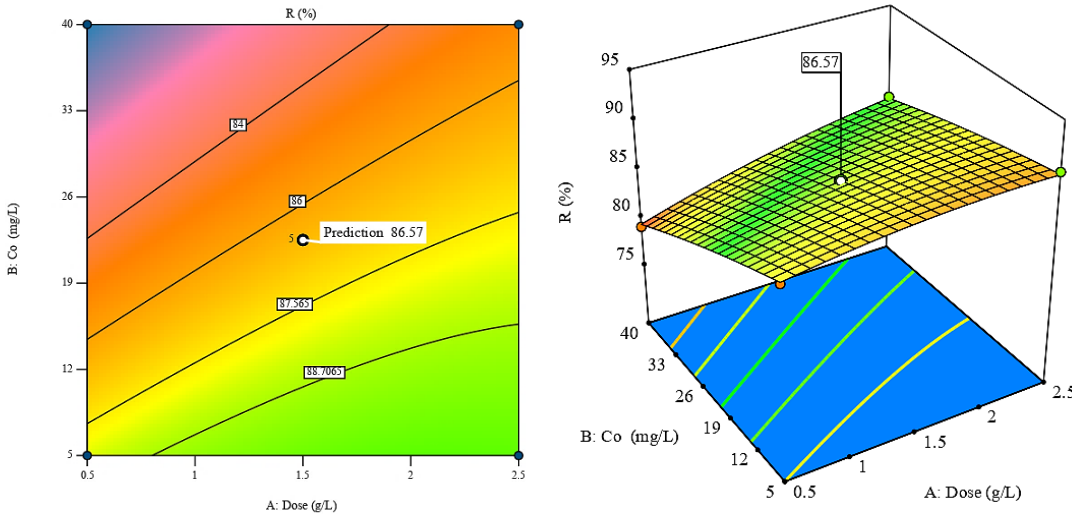


**Figure 9.** Two-dimensional and three-dimensional surface plots showing the  $C_0$  and adsorbent dose on the removal of fluoride by Z-A/M-BC composite.

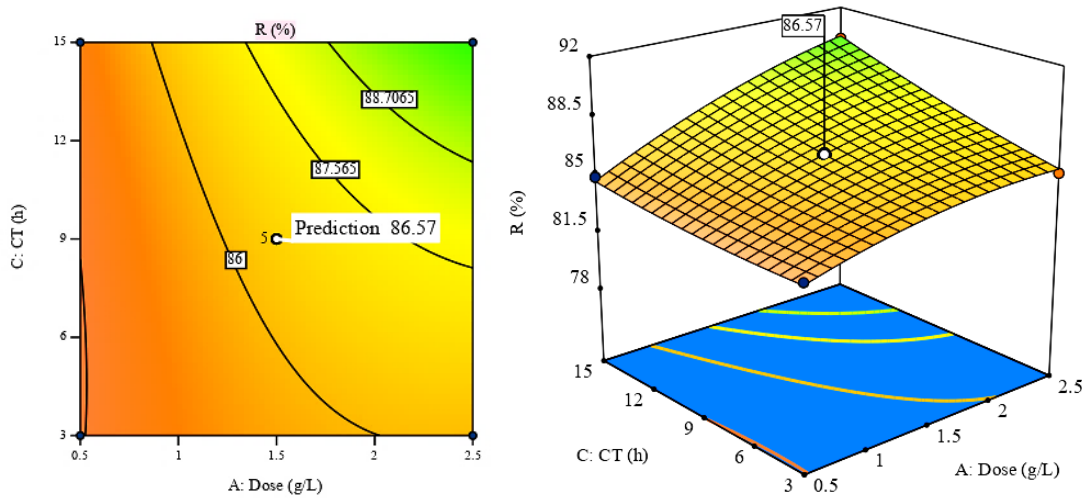


**Figure 10.** Two-dimensional and three-dimensional surface plots showing the effect of adsorbent dose and contact time on the removal of fluoride by Z-A/M-BC composite.

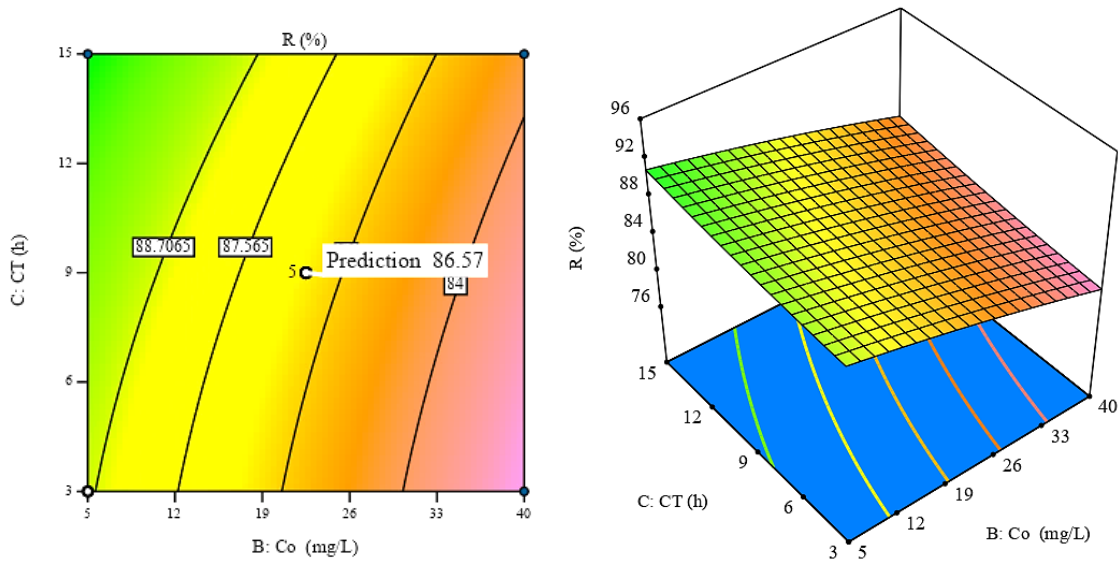


**Figure 11.** Two-dimensional and three-dimensional surface plots showing the impact of  $C_o$  and contact time on the removal of fluoride by Z-A/M-BC composite.

#### Real Sample Analysis and Reusability Test

Before applying the removal test, the content of anions in the groundwater ( $\text{Cl}^-$ ,  $\text{NO}_3^-$ ,  $\text{CO}_3^{2-}$ ,  $\text{SO}_4^{2-}$ , and  $\text{PO}_4^{3-}$ ) was analyzed [20, 51] and the results were tabulated in Table S6. Then the performance of the as-synthesized adsorbent was applied for defluoridation of a real water sample having 12.25 mg/L  $C_o$ , which was collected from Kenteri town, Ethiopia. The equilibrium concentration of fluoride was reduced to 1.35 mg/L (Table S6), which meets the acceptable limit of fluoride concentration in potable water endorsed by WHO [20]. The removal efficiency of synthesized adsorbents (Z-A, BC, M-BC, and Z-A/M-BC) was found to be 46.45%, 51.82%, 44%, and 88.97%, respectively (Fig. 12a). The Z-A/M-BC composite relatively shows better removal efficiency than its pristine materials. However, the Z-A/M-BC composite shows relatively lower removal efficiency in a real water sample than in a simulated water sample. This could be due to the presence of different matrix ions in groundwater (Table S6). The economic viability of the as-synthesized adsorbents was checked by the reusability test. The reusability test of the synthesized Z-A/M-BC composite was found to be 95.80%, 90.40%, 87.30%, 85.40%, and 70.20% removal efficiency for the first, second, third, fourth, and fifth cycles, respectively, which is almost constant removal efficiency from the first to fourth cycles (Fig. 12b).

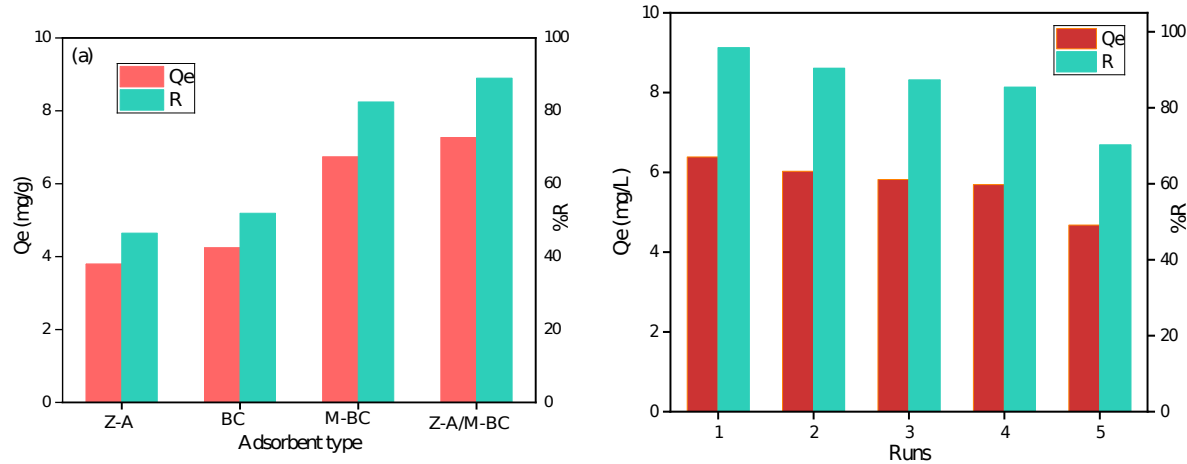


**Fig. 12** Effects of adsorbent nature on the removal efficiency and capacity of Z-A/M-BC (a), and reusability (b).

Comparison of Z-A/M-BC removal efficiency with previous reports

The fluoride removal efficiency of Z-A/M-BC was compared with other adsorbents which was reported previously (Table 1). Accordingly, the synthesized adsorbent shows good defluoridation efficiency. Thus, the finding of this research work suggests that the Z-A/M-BC is a good adsorbent for the defluoridation groundwater.

**Table 1** Comparison of the defluoridation efficiency of Z-A/M-BC composite with Previous Reports.

S. NO	Adsorbents	Removal efficiency (%)	Ref.
1	Fe <sub>3</sub> O <sub>4</sub> /graphene/alginate nanocomposite	85.50%	[42]
2	Lanthanum-doped - activated carbon (AC-La),	92.00%	[2]
3	Zirconia/Zeolite (ZrO <sub>2</sub> -Ze)	94.89%	[346]
4	Activated carbon of <i>Catha edulis</i>	73.00%	[9]
5	Zirconium-MOF (MOF-801)	95.20%	[17]
6	Aluminum hydroxide-loaded zeolite	92.00%	[6]
7	Z-A/M-BC	95.80%	This study

#### Adsorption Mechanisms

The removal mechanism of fluoride via Z-A/M-BC involves surface complexation/precipitation, ion exchange, hydrogen bonding, and electrostatic

interaction (Fig. 13). The hydroxyl groups (M-OH) are substituted by fluoride, and the removal of fluoride proceeds through anion exchange [20]. The defluoridation of fluoride also proceeds via a complexation/precipitation mechanism; fluoride is a hard base that is highly affinized to hard acids ( $\text{Al}^{3+}$ ,  $\text{Fe}^{3+}$ , and  $\text{Si}^{4+}$ ) to form stable products. Most importantly, the defluoridation mechanism occurred via electrostatic interaction on the basis of PZC.

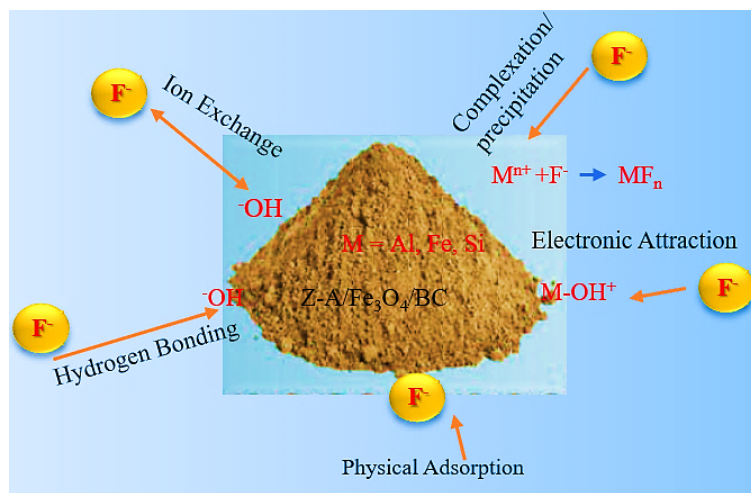


**Fig.13** Proposed removal mechanism of fluoride via Z-A/M-BC composite.

## Conclusions

In the present work, Z-A/M-BC adsorbent was synthesized for the removal of fluoride groundwater. The crystalline size, functional groups, surface area, elemental composition, and morphology of the synthesized Z-A/M-BC composite were also characterized by using PXRD, FT-IR, BET, and SEM-EDX to confirm the formation of adsorbent material. The removal efficiency of Z-A/M-BC adsorbent was started by optimizing pH, adsorbent dose,  $C_o$ , and contact time. The maximum removal efficiency (95.80%) and capacity (6.37 mg/g) were obtained at pH 5, an adsorbent dose of 1.5 g/L, a contact time of 6 h, and  $C_o$  of 10 mg/L. Furthermore, the reusability study was found to be 95.80%, 90.40%, 87.30%, 85.40%, and 70.20% removal efficiency for the first, second, third, fourth, and fifth turns, respectively. This suggests that the Z-A/M-BC composite is efficient and can be reused for the removal of groundwater. The as-synthesized adsorbent was also applied for the defluoridation of a real water sample having 12.25 mg/L fluoride  $C_o$ , which was reduced to 1.35 mg/L, which meets the permissible limit of fluoride concentration in

drinking water recommended by WHO. Thus, the synthesized adsorbent is useful for the removal of fluoride from groundwater.

#### **Author Contributions: CRediT**

**Tessema Derbe:** Writing original draft, Methodology, Data curation, Conceptualization. **Yitayew Tesfaye:** Formal analysis, Data curation. **Taju Sani:** Resources, methodology, Conceptualization. **Enyew Amare Zereffa:** Writing & editing, Supervision, Investigation, Conceptualization.

#### **Data Availability Statement**

Data available upon request from the corresponding author.

#### **Funding Statement**

This work is partly supported by the Addis Ababa Science and Technology University project grant code IG 08/2021.

#### **Statements and Declarations**

The authors declare that they have no known competing financial interests or personal relationships that could have appeared to influence the work reported in this paper.

#### **Acknowledgments**

The authors would like to thank Wachemo University and Addis Ababa Science & Technology University for their providing materials.

#### **References**

- [1] Gómez-Hortigüela L, Pérez-Pariente J, García R, Chebude Y, Díaz I. Natural zeolites from Ethiopia for elimination of fluoride from drinking water. *Sep Purif Technol* 2013; 120:224-9. <https://doi.org/10.1016/j.seppur.2013.10.006>.
- [2] Zhang Y, He L, Wang G, Zhang X, Liu Y, Chen Y. Defluorination and regeneration study of lanthanum-doped sewage sludge-based activated carbon. *J Environ Chem Eng* 2021;9. <https://doi.org/10.1016/j.jece.2021.105740>.
- [3] Chen J, Yang R, Zhang Z, Wu D. Removal of fluoride from water using aluminum hydroxide-loaded zeolite synthesized from coal fly ash. *J Hazard Mater* 2022;421. <https://doi.org/10.1016/j.jhazmat.2021.126817>.

- [4] Dhillon A, Soni SK, Kumar D. Enhanced fluoride removal performance by Ce-Zn binary metal oxide: Adsorption characteristics and mechanism. *J Fluor Chem* 2017; 199: 67-76. <https://doi.org/10.1016/j.jfluchem.2017.05.002>.
- [5] Raghav S, Sapna, Kumar D. Cubical-Shaped Rods of Pectin-Hydroxyapatite Composite for Adsorption Studies of Fluoride by Statistical Method and Adsorption Experiments. *ACS Omega* 2018; 3: 9675-88. <https://doi.org/10.1021/acsomega.8b01330>.
- [6] Chen J, Yang R, Zhang Z, Wu D. Removal of fluoride from water using aluminum hydroxide-loaded zeolite synthesized from coal fly ash. *J Hazard Mater* 2022;421. <https://doi.org/10.1016/j.jhazmat.2021.126817>.
- [7] Teju MD, Majamo SL. Synthesis and application of lanthanum-doped magnetic biochar composite adsorbent for removal of fluoride from water. *Environ Monit Assess* 2023;195. <https://doi.org/10.1007/s10661-023-12075-y>.
- [8] Ebsa DG. Defluoridation of drinking water by modified natural zeolite with Cationic surfactant, in the case of Ziway town, Ethiopia. *Clean Eng Technol* 2023;12. <https://doi.org/10.1016/j.clet.2023.100596>.
- [9] Fito J, Said H, Feleke S, Worku A. Fluoride removal from aqueous solution onto activated carbon of Catha edulis through the adsorption treatment technology. *Environmental Systems Research* 2019; 8. <https://doi.org/10.1186/s40068-019-0153-1>.
- [10] Kamble SP, Dixit P, Rayalu SS, Labhsetwar NK. Defluoridation of drinking water using chemically modified bentonite clay. *Desalination* 2009; 249 :687-93. <https://doi.org/10.1016/j.desal.2009.01.031>.
- [11] Gao Y, Li M, Ru Y, Fu J. Fluoride removal from water by using micron zirconia/zeolite molecular sieve: Characterization and mechanism. *Groundw Sustain Dev* 2021;13. <https://doi.org/10.1016/j.gsd.2021.100567>.
- [12] Afzal, M.Z., Khan, S.A., Song, C. *et al.* Removal of ciprofloxacin via enhancing hydrophilicity of membranes using biochar. *Applied Water Science* 2024; 14:195. <https://doi.org/10.1007/s13201-024-02270-8>
- [13] Sairam Sundaram C, Viswanathan N, Meenakshi S. Defluoridation of water using magnesia/chitosan composite. *J Hazard Mater* 2009; 163: 618-24. <https://doi.org/10.1016/j.jhazmat.2008.07.009>.

- [14] Tabi RN, Agyemang FO, Mensah-Darkwa K, Arthur EK, Gikunoo E, Momade F. Zeolite synthesis and its application in water defluorination. *Mater Chem Phys* 2021;261. <https://doi.org/10.1016/j.matchemphys.2021.124229>.
- [15] Haldar D, Duarah P, Purkait MK. MOFs for the treatment of arsenic, fluoride and iron contaminated drinking water: A review. *Chemosphere* 2020;251. <https://doi.org/10.1016/j.chemosphere.2020.126388>.
- [16] Tan TL, Krusnamurthy PA, Nakajima H, Rashid SA. Adsorptive, kinetics and regeneration studies of fluoride removal from water using zirconium-based metal organic frameworks. *RSC Adv* 2020; 10: 18740-52. <https://doi.org/10.1039/d0ra01268h>.
- [17] Khatamian M, Afshar No N, Hosseini Nami S, Fazli-Shokouhi S. Synthesis and characterization of zeolite A, Fe<sub>3</sub>O<sub>4</sub>/zeolite A, and Fe<sub>2</sub>O<sub>3</sub>/zeolite A nanocomposites and investigation of their arsenic removal performance. *Journal of the Iranian Chemical Society* 2023; 20: 1657-70. <https://doi.org/10.1007/s13738-023-02787-w>.
- [18] Derbe T, Zereffa EA, Sani T. Synthesis of zeolite-A/Fe<sub>3</sub>O<sub>4</sub>/biochar composite for removal of Cr(VI) from aqueous solution. *International Journal of Environmental Science and Technology* 2024. <https://doi.org/10.1007/s13762-024-05642-4>.
- [19] Sani T, Gómez-Hortigüela L, Pérez-Pariente J, Chebude Y, Díaz I. Defluoridation performance of nano-hydroxyapatite/stilbite composite compared with bone char. *Sep Purif Technol* 2016;157:241-8. <https://doi.org/10.1016/j.seppur.2015.11.014>.
- [20] Derbe, T., Gindose, T.G., Sani, T. Enyew Amare Zereffa. EA. Synthesis of zeolite-A/Fe<sub>3</sub>O<sub>4</sub>/biochar/MOF-5 composite for the defluoridation of drinking water. *Applied Water Science* 2025; 15: 161. <https://doi.org/10.1007/s13201-025-02438-w>
- [21] Zhou N, Guo X, Ye C, Yan L, Gu W, Wu X, et al. Enhanced fluoride removal from drinking water in wide pH range using La/Fe/Al oxides loaded rice straw biochar. *Water Supply* 2022; 22: 779-94. <https://doi.org/10.2166/ws.2021.232>.
- [22] Zheng XJ, Chen M, Wang JF, Liu Y, Liao YQ, Liu YC. Assessment of zeolite, biochar, and their combination for stabilization of multmetal-contaminated soil. *ACS Omega* 2020; 5: 27374-82. <https://doi.org/10.1021/acsomega.0c03710>.
- [23] Zhang J, Lin S, Han M, Su Q, Xia L, Hui Z. Adsorption properties of magnetic magnetite nanoparticle for coexistent Cr(VI) and Cu(II) in mixed solution. *Water (Switzerland)* 2020; 12. <https://doi.org/10.3390/w12020446>.
- [24] Shemy MH, Othman SI, Alfassam HE, Al-Waili MA, Alqhtani HA, Allam AA, et al. Synthesis of Green Magnetite/Carbonized Coffee Composite from Natural Pyrite for

Effective Decontamination of Congo Red Dye: Steric, Synergetic, Oxidation, and Ecotoxicity Studies. *Catalysts* 2023;13. <https://doi.org/10.3390/catal13020264>.

- [25] Tran NBT, Duong NB, Le NL. Synthesis and Characterization of Magnetic  $\text{Fe}_3\text{O}_4$ /Zeolite NaA Nanocomposite for the Adsorption Removal of Methylene Blue Potential in Wastewater Treatment. *J Chem* 2021;2021. <https://doi.org/10.1155/2021/6678588>.
- [26] Khatamian M, Afshar No N, Hosseini Nami S, Fazli-Shokouhi S. Synthesis and characterization of zeolite A,  $\text{Fe}_3\text{O}_4$ /zeolite A, and  $\text{Fe}_2\text{O}_3$ /zeolite A nanocomposites and investigation of their arsenic removal performance. *Journal of the Iranian Chemical Society* 2023; 20:1657-70. <https://doi.org/10.1007/s13738-023-02787-w>.
- [27] Saeed AAH, Harun NY, Sufian S, Bilad MR, Zakaria ZY, Jagaba AH, et al. Pristine and magnetic kenaf fiber biochar for  $\text{Cd}^{2+}$  adsorption from aqueous solution. *Int J Environ Res Public Health* 2021;18. <https://doi.org/10.3390/ijerph18157949>.
- [28] Vo AT, Nguyen VP, Ouakouak A, Nieva A, Doma BT, Tran HN, et al. Efficient removal of Cr(VI) from water by biochar and activated carbon prepared through hydrothermal carbonization and pyrolysis: Adsorption-coupled reduction mechanism. *Water (Switzerland)* 2019;11. <https://doi.org/10.3390/w11061164>.
- [29] Assirey EA, Altamimi LR. Chemical analysis of corn cob-based biochar and its role as water decontaminants. *Journal of Taibah University for Science* 2021; 15: 111-21. <https://doi.org/10.1080/16583655.2021.1876350>.
- [30] Ghaffar A, Zhu X, Chen B. Biochar composite membrane for high performance pollutant management: Fabrication, structural characteristics and synergistic mechanisms. *Environmental Pollution* 2018; 233:1013-23. <https://doi.org/10.1016/j.envpol.2017.09.099>.
- [31] Fito J, Abewaa M, Nkambule T. Magnetite-impregnated biochar of parthenium hysterophorus for adsorption of Cr(VI) from tannery industrial wastewater. *Appl Water Sci* 2023;13. <https://doi.org/10.1007/s13201-023-01880-y>.
- [32] Pan X, Gu Z, Chen W, Li Q. Preparation of biochar and biochar composites and their application in a Fenton-like process for wastewater decontamination: A review. *Science of the Total Environment* 2021;754. <https://doi.org/10.1016/j.scitotenv.2020.142104>.
- [33] Mosa A, El-Ghamry A, Tolba M. Biochar-supported natural zeolite composite for recovery and reuse of aqueous phosphate and humate: Batch sorption-desorption

and bioassay investigations. Environ Technol Innov 2020;19. <https://doi.org/10.1016/j.eti.2020.100807>.

- [34] Kong F, Zhang Y, Wang H, Tang J, Li Y, Wang S. Removal of Cr(VI) from wastewater by artificial zeolite spheres loaded with nano Fe-Al bimetallic oxide in constructed wetland. Chemosphere 2020;257. <https://doi.org/10.1016/j.chemosphere.2020.127224>.
- [35] Kosmulski M. The pH dependent surface charging and points of zero charge. IX. Update. Adv Colloid Interface Sci 2021;296. <https://doi.org/10.1016/j.cis.2021.102519>.
- [36] Gao Y, Li M, Ru Y, Fu J. Fluoride removal from water by using micron zirconia/zeolite molecular sieve: Characterization and mechanism. Groundw Sustain Dev 2021;13. <https://doi.org/10.1016/j.gsd.2021.100567>.
- [37] Tolkou AK, Zouboulis AI. Fluoride Removal from Water Sources by Adsorption on MOFs. Separations 2023;10. <https://doi.org/10.3390/separations10090467>.
- [38] Tabi RN, Agyemang FO, Mensah-Darkwa K, Arthur EK, Gikunoo E, Momade F. Zeolite synthesis and its application in water defluorination. Mater Chem Phys 2021;261. <https://doi.org/10.1016/j.matchemphys.2021.124229>.
- [39] Hussein IA, Vegi MR. Defluoridation of drinking water using coalesced and uncoalesced mica. Appl Water Sci 2020;10. <https://doi.org/10.1007/s13201-020-1153-z>.
- [40] Jung KW, Choi BH, Jeong TU, Ahn KH. Facile synthesis of magnetic biochar/Fe<sub>3</sub>O<sub>4</sub> nanocomposites using electro-magnetization technique and its application on the removal of acid orange 7 from aqueous media. Bioresour Technol 2016; 220: 672-6. <https://doi.org/10.1016/j.biortech.2016.09.035>.
- [41] Ahmad M, Ahmad M, Usman ARA, Al-Faraj AS, Abduljabbar A, Ok YS, et al. Date palm waste-derived biochar composites with silica and zeolite: synthesis, characterization and implication for carbon stability and recalcitrant potential. Environ Geochem Health 2019; 41:1687-704. <https://doi.org/10.1007/s10653-017-9947-0>.
- [42] Kumari S, Singh N, Sharma R, Yadav M, Khan S. Kinetics and isotherms of adsorption of fluoride onto Fe<sub>3</sub>O<sub>4</sub>/graphene/alginate nanocomposite hydrogel. Environ Nanotechnol Monit Manag 2021;16. <https://doi.org/10.1016/j.enmm.2021.100590>.

- [43] Santhosh C, Daneshvar E, Tripathi KM, Baltrénas P, Kim TY, Baltrénaitė E, et al. Synthesis and characterization of magnetic biochar adsorbents for the removal of Cr(VI) and Acid orange 7 dye from aqueous solution. *Environmental Science and Pollution Research* 2020; 27: 32874-87. <https://doi.org/10.1007/s11356-020-09275-1>.
- [44] Cao J, Sun Q, Wang P, Shen J, Dai X. Synthesize and characterize of  $\text{Fe}_3\text{O}_4$ /zeolite 4A magnetic nanocomposite. *J Dispers Sci Technol* 2022; 43:517-25. <https://doi.org/10.1080/01932691.2020.1843480>.
- [45] Ayele Regassa L. Synthesis and Characterization of Zeolite A from Kaolin of Ethiopia: Studies of its application as detergent builder and in tannery wastewater treatment. 2016.
- [46] Belachew N, Hinsene H. Preparation of Zeolite 4A for Adsorptive Removal of Methylene Blue: Optimization, Kinetics, Isotherm, and Mechanism Study. *Silicon* 2022; 14: 1629-41. <https://doi.org/10.1007/s12633-020-00938-9>.
- [47] Kokab T, Ashraf HS, Shakoor MB, Jilani A, Ahmad SR, Majid M, et al. Effective removal of Cr(Vi) from wastewater using biochar derived from walnut shell. *Int J Environ Res Public Health* 2021;18. <https://doi.org/10.3390/ijerph18189670>.
- [48] Kamble SP, Dixit P, Rayalu SS, Labhsetwar NK. Defluoridation of drinking water using chemically modified bentonite clay. *Desalination* 2009; 249: 687-93. <https://doi.org/10.1016/j.desal.2009.01.031>.
- [49] Sairam Sundaram C, Viswanathan N, Meenakshi S. Defluoridation of water using magnesia/chitosan composite. *J Hazard Mater* 2009; 163: 618-24. <https://doi.org/10.1016/j.jhazmat.2008.07.009>.
- [50] Dhillon A, Soni SK, Kumar D. Enhanced fluoride removal performance by Ce-Zn binary metal oxide: Adsorption characteristics and mechanism. *J Fluor Chem* 2017; 199: 67-76. <https://doi.org/10.1016/j.jfluchem.2017.05.002>.
- [51] Massoudinejad M, Ghaderpoori M, Shahsavani A, Amini MM. Adsorption of fluoride over a metal organic framework Uio-66 functionalized with amine groups and optimization with response surface methodology. *J Mol Liq* 2016; 221:279-86. <https://doi.org/10.1016/j.molliq.2016.05.087>.
- [52] Behailu TW, Badessa TS, Tewodros BA. Analysis of physical and chemical parameters in ground water consumed within Konso area, Southwestern Ethiopia. *Afr J Environ Sci Tech* 2018; 12: 106-14. <https://doi.org/10.5897/ajest2017.2419>.